Sol-Gel Preparation of Layered δ-MnO_2 Phase for Salt Removal by Hybrid Capacitive Deionization

M. D. To[1,2], H. A. Nguyen[1,2], T. A. Dao[1,2], T. N. K. Nguyen[1,2], V. V. Nguyen[1,2], T. H. Nguyen[1,2], V. H. Le[1,2] and L. T. N. Huynh[1,2]

[1]*Vietnam National University of Ho Chi Minh City, Vietnam*
[2]*University of Science, Ho Chi Minh City, Vietnam*
Corresponding author: hltnguyen@hcmus.edu.vn

Received 20/07/2024; accepted 05/01/2025
https://doi.org/10.4152/pea.2026440603

Abstract
Recent research on capacitive deionization (CDI) materials indicates that salt removal efficiency of their cells can be increased by modifying one carbon electrode, with an electrode operating through a redox mechanism. A potential candidate is δ-MnO_2, due to its diverse crystalline phase structure, low price and environmental friendliness. This study synthesized the layered phase of δ-MnO_2 via sol-gel route, targeting a high-performance electrode for hybrid CDI (HCDI) technology. Analyzes results on δ-MnO_2 composition and porosity were verified through BET, Raman, SEM and X-RD measurements. Electrochemical properties confirmed pseudo-capacitance charge-storage of δ-MnO_2 and high durability, with specific capacitance (C_{sp}) of 143 F/g, at a rate of 1 A/g, remaining stable after 1000 cycles. Efficiency of salt removal by optimal performance active material, at 1.4 V, with a moderate salt adsorption capacity (SAC) of 22.5 mg/g, was investigated.

Keywords: δ-MnO_2; HCDI; pseudo-capacitance; SAC; water desalination.

Introduction•

Capacitive deionization (CDI) is a promising desalination technology that provides advantages in terms of efficiency, energy savings, durability, low cost and environmental friendliness for water treatment [1]. Primary CDI consists of two porous carbon electrodes that adsorb ions in water through an electric double-layer mechanism. To achieve conditions for features such as high porosity, large surface area and low price, some recent studies on synthesizing carbon from many sources, such as using activated carbon made from coconut shells, have shown that average salt adsorption capacity (SAC) was around 10 mg/g [2-4], and that carbon aerogel from resorcinol and formaldehyde resulted in a SAC of 10.34 mg/g [5-7].
However, poor electrical conductivity of carbon materials poses a drawback for CDI technology, and requires improvement to enhance desalination capabilities. In recent years, research has indicated that salt removal efficiency of CDI cells can

•The abbreviations list is in page 426.

be increased by modifying one of the carbon electrodes with an electrode operating through a redox mechanism - a method referred to as hybrid CDI (HCDI). Redox electrodes of HCDI will eliminate ions in the solution through charge transfer process, involving intercalation of ions from the solution into the crystalline structure of the active material. Consequently, salt removal is no longer constrained by the surface area of the material within the electrode [8]. Some examples of metal oxides used as cathode electrodes of CDI cells are MnO_2, SnO_2 TiO_2 and ZnO, [9-17]. Among these, TiO_2 and MnO_2 possess the advantages of being cost-effective, environmentally friendly, and exhibiting high physical and chemical durability.

In particular, MnO_2 has a variety of phases, including crystalline and amorphous ones. Crystalline phases of MnO_2, from α- to γ-phases, are made up of MnO_6 octahedral units that share corners or edges, causing them to form different tunnel and layer structures. To explore the suitability and desalination efficacy of different MnO_2 crystal phases, this study concentrates on delta crystal form of MnO_2 (δ-MnO_2) characterized by a 2D structure. This choice was motivated by unique electrochemical properties stemming from the material's layered structure. The layered arrangement facilitates ingress and interweaving of ions throughout each crystalline layer, contributing to enhanced desalination capabilities.

This research explored the synthesis of δ-MnO_2, using a sol-gel method to evaluate electrochemical properties and effectiveness in hybrid capacitive deionization systems for water desalination. This structure exhibited a promising CDI performance in asymmetric AC|| δ-MnO_2, obtaining an impressive 22.5 mg/g salt removal.

Experimental

Synthesis of δ-MnO_2 phase

In this study, MnO_2 material was synthesized using sol-gel method. MnO_2 was prepared by reducing $KMnO_4$ with fumaric acid mixed in the mole ratio 3:1, stirring slowly, and heating until $C_4H_4O_4$ completely dissolved [18]. $KMnO_4$ solution was slowly added drop by drop into the Becher containing $C_4H_4O_4$, while stirring. Temperature was maintained at 80 °C, until sol became a gel. The gel was dried at 120 °C, for 1 h and 30 min, to obtain a powder product. The powder was finely ground and calcined at 600 °C air conditions, for 12 h. Then, the product was treated with 2 M H_2SO_4, by stirring it for 30 min. Then, it was washed several times with water, until it reached neutral pH. The final powder product was filtered and dried at 120 °C, overnight.

Structural and morphological characterization

The δ-MnO_2 phase was analyzed by X-RD method, on a D8-Advance diffractometer (Bruker) equipped with LYNSEYES detector, with a Cu anode (λK_α = 1.54180 Å), in a scanning angle range from 10 to 80º (0.02º/step). Raman spectroscopy analysis was conducted in a range from 100 to 1000 cm^{-1}, at ambient temperature, using a

785-nm laser-equipped XploRA HORIBA confocal microscope, as excitation source. Pore structure and surface properties were analyzed using analytical method Brunauer – Emmett – Teller (BET), a nitrogen adsorption-desorption isotherm measured at 77 K.

Electrochemical and desalination characterization

Electrochemical properties of the electrode material were investigated using a three-electrode system: working and reference electrodes were Ag/AgCl (3.5 M KCl), and counter electrode was Pt in a 1 M Na_2SO_4 electrolyte solution on a Gamry Reference 600, USA. EIS method was measured from 100 kHz to 0.1 Hz, and CV was performed in the window voltage from 0 to 1.0 V (*v.* Ag/AgCl), at scan rates from 5 to 100 mV/s. CDI batch mode measurements were conducted to evaluate salt removal performance using a peristaltic pump, asymmetric CDI cell as AC||δ-MnO_2, current pressure and conductivity meters (Jenway 4510). A 200 ppm NaCl solution with a fixed volume of 30 mL, with a constant applied potential of 1.0, 1.2, 1.4 and 1.6 V.

Results and discussion

Structural and morphological characterization

X-RD pattern of δ-MnO_2 is depicted in Fig. 1a, where the most pronounced diffraction lines are aligned with (001) planes, corresponding to Birnessite-type structure, with a lamellar stack and monoclinic symmetry (C2/m) [19, 20]. It was well defined by cell parameters with: a, b and c of 4.9253, 2.8345 and 7.1384 Å, respectively. β was 103.2º.

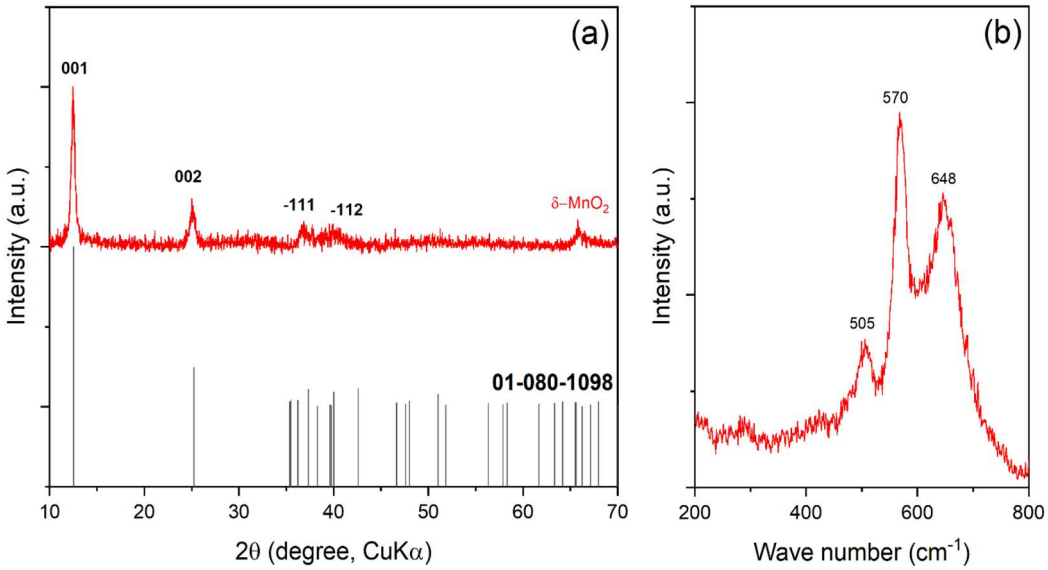

Figure 1: (a) XRD pattern sample of δ-MnO; **(b)** Raman scattering (RS) spectra of δ-MnO_2.

Fig.1a clearly shows a significant preferential orientation, as evidenced by the exclusive prominence of (001) and (002) peaks. The intensity of these peaks suggests a stacking of the layers along (a, b) plane across extensive domains.

Fig. 1b depicts Raman spectrum of δ-MnO_2, showing distinct peaks associated with specific vibrational modes of MnO_2 structure. The peak around 570 cm^{-1} is assigned to Mn-O stretching mode of MnO_6 octahedra. This mode is characteristic of MnO_2framework, and the specific frequency provides information about the nature of the bonding and structure. The peaks at 505 and 648 cm^{-1} have been mentioned as being potentially related to other vibrational modes within MnO_2 structure, which may include Mn-O-Mn bending and stretching modes [21, 22].
Nitrogen adsorption-desorption isotherm, at 77 K, for δ-MnO_2, in Figure 2, significantly reveals Type IV pattern, with a distinct hysteresis loop, indicating a mesoporous structure with uniform pore sizes. The surface area following BET was calculated at 120 m^2/g. Hysteresis loop shape suggests that mesopores may be of a uniform shape, which is advantageous for consistent transport and charge-storage properties.

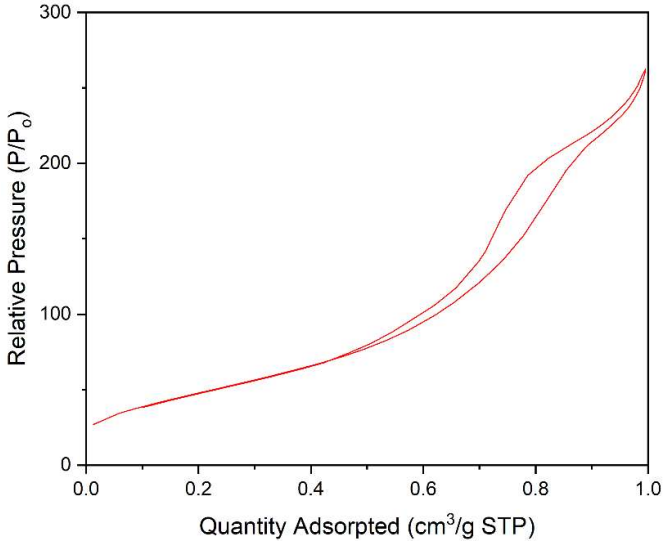

Figure 2: Nitrogen adsorption-desorption isotherm, measured at 77 K, for δ-MnO_2.

Figure 3a offers an overview of δ-MnO_2 morphology at 5k magnification; one observes a heterogeneous, highly porous and polydisperse structure typical for MnO_2. SEM images in higher magnification (10 and 15k, in Figure 3b-c) show particles size in the range of sub-micro scale, from 0.5 to 0.7 µm. Surface roughness and interconnected pore structure through small particle aggregation suggest facile ion penetration and high active sites for redox reaction.

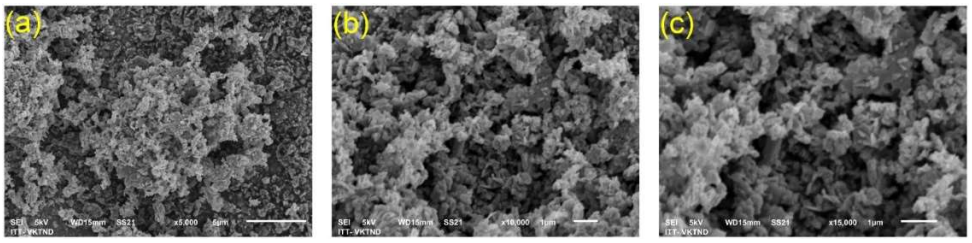

Figure 3. SEM images of δ-MnO_2 at various magnifications: **(a)** 5, **(b)** 10 and **(c)** 15k.

Electrochemical and desalination performance

Electrochemical properties of δ-MnO_2 were studied through CV and EIS. Figure 4a shows CV curves of δ-MnO_2, at different scan rates, in a 1.0 M Na_2SO_4 solution. At slow voltage rates from 5 to 25 mV/s, CV have a roughly rectangular shape, since they cannot keep perfect curves when scanning speed is greater than 50 mV/s, which is proven by specific capacitance (C_{sp}) results in Figure 4b.

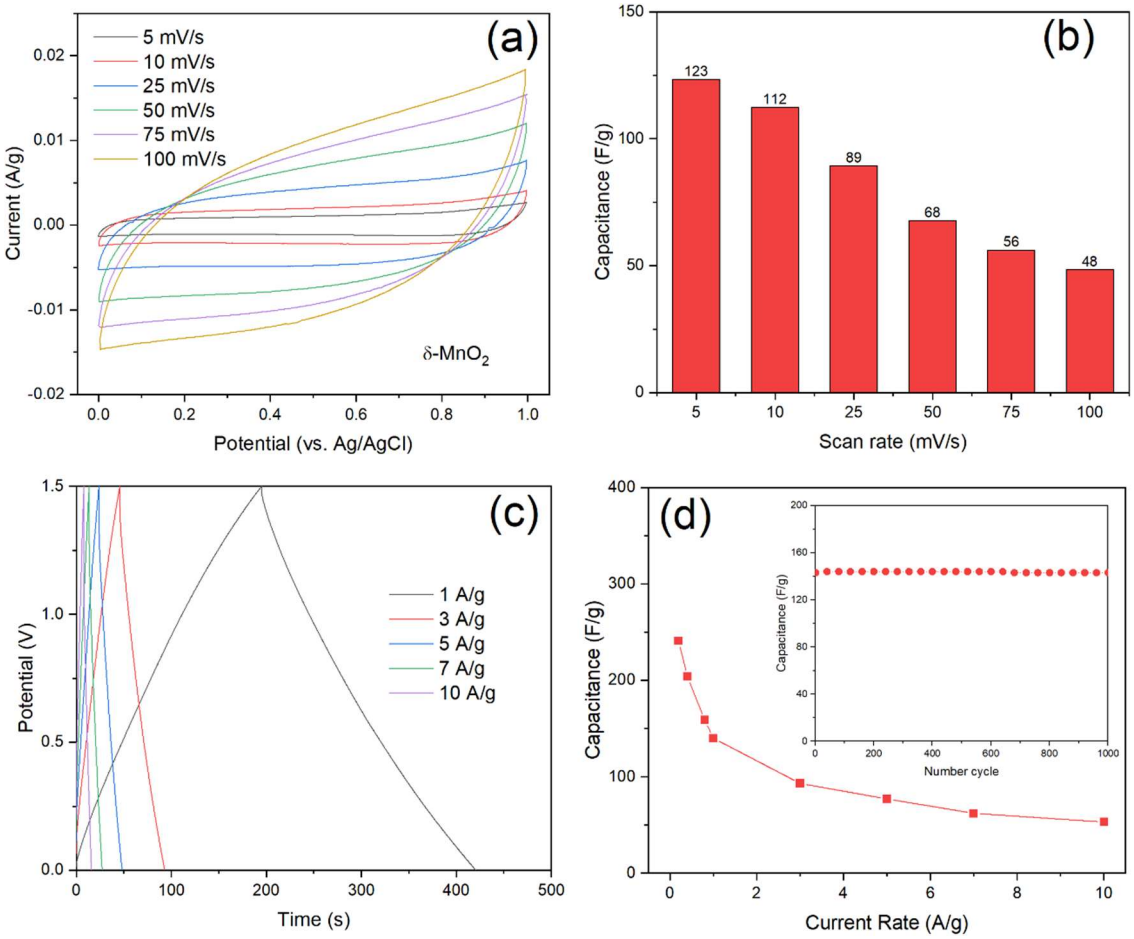

Figure 4: (a) CV curves at different scan rates, with potential from 0 to1.5 V; **(b)** capacitance at different scan rates; **(c)** galvanostatic charge-discharge curves at different current densities; and **(d)** cycling stability upon to 1000 cycles, and capacitance in different current densities of δ-MnO_2 electrode.

Highest C_{sp} was calculated to be 123 F/g at the lowest scan rate, 5 mV/s. It reduced by about half, to 68 F/g, when reaching a scan rate of 50 mV/s. At the two highest scanning speeds studied, 75 and 100 mV/s, the decrease in C_{sp} slowed down, giving results of 56 and 48 F/g, respectively. The reduction in capacitance indicates limited ion diffusion when potential changed rapidly, as there may be insufficient time for ions to move in and out of the electrode's pores and surface.

Figure 4c shows charge-discharge profile of δ-MnO_2, at different current densities, from 1 to 10 A/g, exhibiting a triangular shape without discernible IR drop, which is characteristic of pseudo-capacitive behavior with a symmetrical charge-

discharge profile. Highest C_{sp} result, at the lowest current density of 1 A/g, was nearly 250 F/g. At a current density of 10 A/g, C_{sp} value was close to 143 F/g. Good stable performance of δ-MnO_2 electrode was verified in 1000 cycles, as shown in the inset in Figure 4d. Capacitance stabilization indicates that δ-MnO_2 achieved a steady state where electrochemical processes became reversible. The fact that the discharge curves maintained their shape across various current rates suggests that δ-MnO_2 can deliver consistent performance over different operational conditions, which is advantageous for supercapacitor and capacitive deionization applications.

EIS results in Nyquist plot of δ-MnO_2 electrode in 1 M Na_2SO_4 were measured in the frequency range from 100 kHz to 0.1 Hz, with the excitation signal of 5 mV peak-to-peak. As shown in Figure 5a, the diameter of the semicircle at the high-frequency region coincides with charge transfer resistance. The slope line at intermediate frequencies illustrates Warburg impedance related to the ions' diffusion within the electrode material. The transition from the semicircle to the Warburg region shows that charge transfer and diffusion processes controlled electrochemical behavior of δ-MnO_2 [23-24]. At low frequencies, linear slope increased over 45°, due to electrolyte penetration into pore size structure. Figure 5b shows a linear relationship between Z' and $\omega^{-1/2}$ plot, suggesting a diffusion-controlled process. The straight line with a slope of 49.7 Ω/$s^{1/2}$ confirms that ion transport within the electrode followed Warburg-type diffusion, which has a high correlation coefficient (R^2 = 0.999). From there, it was possible to calculate ionic diffusion coefficient of 7.26 × $10^{-16}$$cm^2$/s.

Desalination performance of δ-MnO_2 electrode was studied through batch-mode HCDI experiments, with different cell voltages of 1.0, 1.2, 1.4 and 1.6 V. Fig. 5a shows absorption curve of δ-MnO_2 electrode via a 200 mg/L NaCl solution, in 60 min.

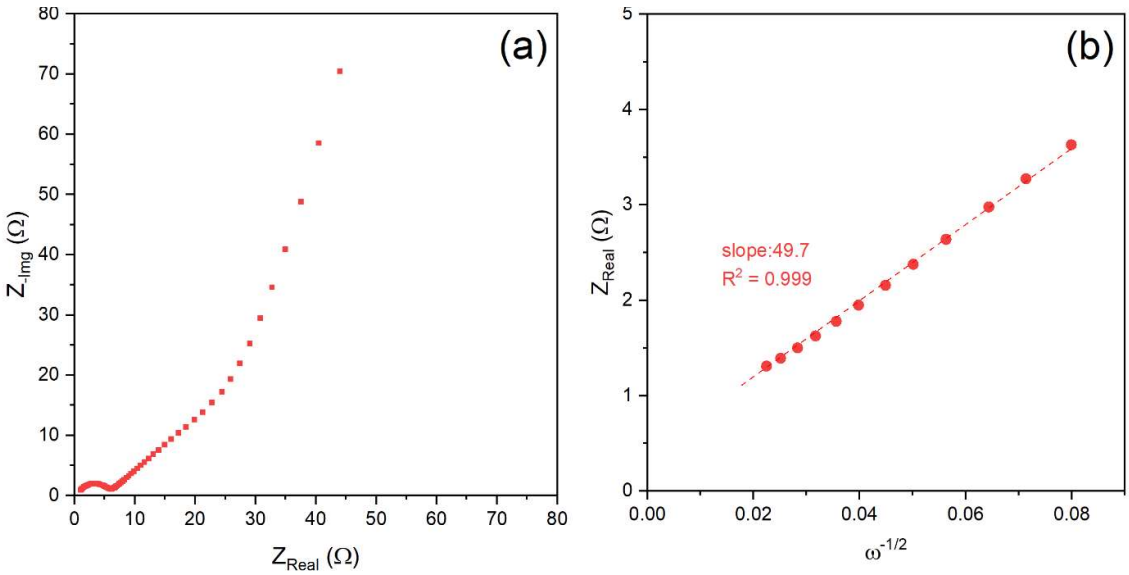

Figure 5: Nyquist plot for **(a)** δ-MnO_2 and **(b)** Z' vs. $\omega^{-1/2}$ plot.

Whatever the applied potential, a quick decrease in NaCl content was observed, suggesting high-rate absorption. Saturation was reached at approximately 30 min, and 1.4 V potential showed the lowest salt concentration, after 60 min, leading to the highest salt removal. In addition, CDI Ragone graph in Fig. 5b demonstrates that, at a voltage of 1.4 V, deionization capacity and average deionization rate are highest at the upper and right regions of the graph. At 1.6 V, it is only seen that graph shift region was at the top, and did not change much on the right side. SAC of δ-MnO_2 electrodes in different constant applied potentials are shown in Fig. 5c. The 1.4 V potential displayed highest SAC (22.5 mg/g). Among all potentials, SAC values were 8.4, 11.1 and 13.4 mg/g, for 1.0, 1.2 and 1.6 V, respectively. Therefore, results show that δ-MnO_2 electrode operated optimally at an applied potential of 1.4 V (Fig. 6).

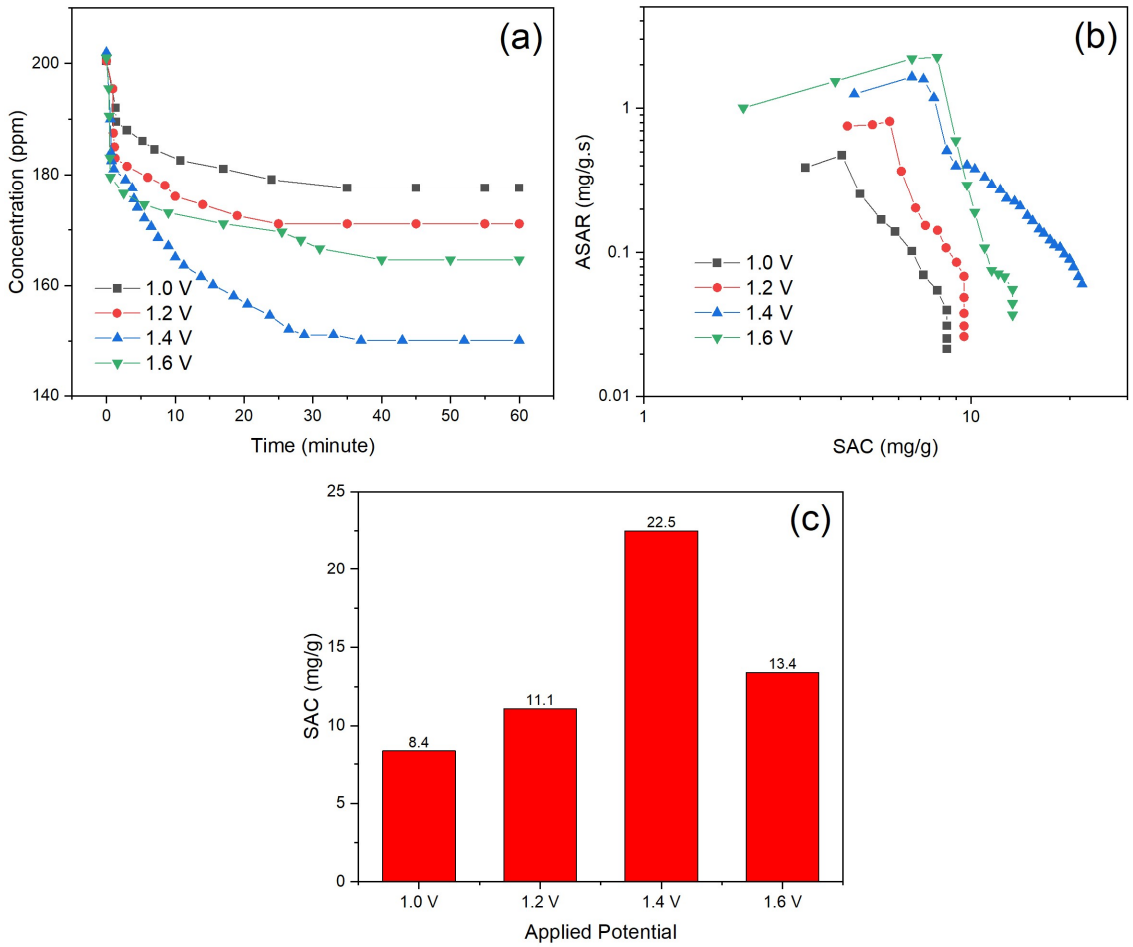

Figure 6: (a) CDI performance; **(b)** CDI Ragone plot; and **(c)** SAC of δ-MnO_2 electrode in a 200 mg/L NaCl solution with various applied potentials.

Conclusion

This research has successfully demonstrated the synthesis of δ-MnO_2 via sol-gel route, highlighting its potential to enhance the efficiency of HCDI systems. The layered phase δ-MnO_2, characterized by its unique structural and electrochemical properties, has shown high specific surface area and stable performance over 1000 cycles, underscoring its suitability for water desalination applications and potential

integration into supercapacitor technology. In CDI performance, δ-MnO_2 exhibited promising results in salt removal efficiency, at an optimal voltage of 1.4 V, with encouraging SAC of 22.5 mg/g, and ASAR above 1 mg/g/s. Future work should focus on optimizing the synthesis process to enhance electrochemical properties of δ-MnO_2 further exploring its applicability in other environmental and energy storage applications, and evaluating long-term stability and scalability of the developed materials for commercial use.

Authors' contributions

M. D. To and H. A. Nguyen: writing – original draft, review and editing; data curation. **M. D. To, T. A. Dao and V. H. Le**: investigation; data curation; visualization. **T. N. K. Nguyen, V. V. Nguyen and T. H. Nguyen**: methodology; visualization. **V. H. Le**: writing – review. **L. T. N. Huynh**: project administration; funding acquisition; resources; supervision; writing – review.

Conflicts of interest

The authors declare that there is no conflict of interest.

Acknowledgment

This research was funded by Vietnam National University Ho Chi Minh City (VNUHCM) under grant number B2023-18-07.

Abbreviations

δ-MnO_2: delta manganese dioxide (Birnessite)
BET: Brunauer-Emmett-Teller
C: carbon
CDI: capacitive deionization
C_{sp}: specific capacitance
CV: cyclic voltammetry
EIS: electrochemical impedance spectroscopy
HCDI: hybrid capacitive deionization
Na_2SO_4: sodium sulfate
Redox: reduction-oxidation reactions
SAC: salt absorption capacity
SEM: scanning electron microscopy
X-RD: X-ray diffraction

References

1. Chen Y-W, Chen J-F, Lin C-H et al. Integrating a supercapacitor with capacitive deionization for direct energy recovery from the desalination of brackish water. Appl Energy. 2019;252:113417. https://doi.org/10.1016/j.apenergy.2019.113417

2. Huynh LTN, Pham TN, Nguyen TH. Coconut shell-derived activated carbon and carbon nanotubes composite: a promising candidate for capacitive deionization electrode. Synth Met. 2020;265:116415. https://doi.org/10.1016/j.synthmet.2020.116415
3. Le VH, Huynh LTN, Tran TN et al. Comparative desalination performance of activated carbon from coconut shell waste/carbon nanotubes composite in batch mode and single-pass mode. J Appl Electrochem. 2021;51:1313-1322. https://doi.org/10.1007/s10800-021-01575-9
4. Huynh LNT, Tran TN, Ho TNT et al. Fabrication of composited electrode based on coconut activated carbon and MCNTs for ionic electrosorption. Viet J Catal Adsor. 2023;12:60-67. https://doi.org/10.51316/jca.2023.010
5. Zhang C, Wang X, Wang H et al. A positive-negative alternate adsorption effect for capacitive deionization in nano-porous carbon aerogel electrodes to enhance desalination capacity. Desalination. 2019;458:45-53. https://doi.org/10.1016/j.desal.2019.01.023
6. Nguyen TVT, Nguyen NT, Nguyen VV et al. Effect of Urea Content on MCDI Performance of Waste-Corn-Stalk-Derived Cellulose Carbon Aerogel. Fib Polym. 2023;24:1929-1939. https://doi.org/10.1007/s12221-023-00234-4
7. Nguyen TH, Nguyen VV, Nguyen NT et al. Preparation, characterization and CDI application of KOH-activated porous waste-corn-stalk-based carbon aerogel. J Por Mat. 2023;30:1183-1193. https://doi.org/10.1007/s10934-022-01411-1
8. Agartan L, Hayes-Oberst B, Byles BW et al. Influence of operating conditions and cathode parameters on desalination performance of hybrid CDI systems. Desalination. 2019;452:1-8. https://doi.org/10.1016/j.desal.2018.10.025
9. Kim C, Lee J, Kim S et al. TiO_2 sol–gel spray method for carbon electrode fabrication to enhance desalination efficiency of capacitive deionization. Desalination. 2014;342:70-74. https://doi.org/10.1016/j.desal.2013.07.016
10. Feng J, Xiong S, Wang Y. Atomic layer deposition of TiO_2 on carbon-nanotube membranes for enhanced capacitive deionization. Sep Purif Technol. 2019;213:70-77. https://doi.org/10.1016/j.seppur.2018.12.026
11. Nguyen LTT, Nguyen TT, Nguyen HA et al. Fabrication of TiO_2 /CNTs composite electrode with improved performance in capacitive deionization. Clean (Weinh). 2023;52:2300037. https://doi.org/10.1002/clen.202300037
12. Yasin AS, Hyun KD, Lee K. One-pot synthesis of activated carbon decorated with ZnO nanoparticles for capacitive deionization application. J Alloys Compd. 2021;870:159422. https://doi.org/10.1016/j.jallcom.2021.159422
13. Laxman K, Myint MTZ, Khan R et al. Improved desalination by zinc oxide nanorod induced electric field enhancement in capacitive deionization of brackish water. Desalination. 2015;359:64-70. https://doi.org/10.1016/j.desal.2014.12.029

14. Xie K, Yu J, Zhang X et al. Capacitive desalination of a low concentration aqueous sodium chloride solution based on a SnO_2 and polystyrene co-functionalized graphene oxide electrodes. Chem Eng J. 2021;414:128747. https://doi.org/10.1016/j.cej.2021.128747
15. Wang S, Wang S, Wang G. Ion removal performance and enhanced cyclic stability of SnO_2/CNT composite electrode in hybrid capacitive deionization. Mater Today Commun. 2020;23:100904. https://doi.org/10.1016/j.mtcomm.2020.100904
16. Hand S, Cusick RD. Characterizing the Impacts of Deposition Techniques on the Performance of MnO_2 Cathodes for Sodium Electrosorption in Hybrid Capacitive Deionization. Environ Sci Technol. 2017;51:12027-12034. https://doi.org/10.1021/acs.est.7b03060
17. Tan G, Lu S, Xu N et al. Pseudocapacitive Behaviors of Polypyrrole Grafted Activated Carbon and MnO_2 Electrodes to Enable Fast and Efficient Membrane-Free Capacitive Deionization. Environ Sci Technol. 2020;54:5843-5852. https://doi.org/10.1021/acs.est.9b07182
18. Bach S, Pereira-Ramos JP, Baffier N. Electrochemical sodium insertion into the sol-gel birnessite manganese dioxide. Electrochim Acta. 1993;38:1695-1698. https://doi.org/10.1016/0013-4686(93)85063-5
19. Franger S, Bach S, Farcy J et al. Synthesis, structural and electrochemical characterizations of the sol–gel birnessite $MnO_{1.84}\cdot 0.6H_2O$. J Pow Sour. 2002;109:262-275. https://doi.org/10.1016/S0378-7753(02)00072-1
20. Franger S, Bach S, Pereira-Ramos JP et al. Highly rechargeable $Li_xMnO_{2+\delta}$ oxides synthesized via low temperatures techniques. J Pow Sour. 2001;97-98:344-348. https://doi.org/10.1016/S0378-7753(01)00725-X
21. Julien C. Raman spectra of birnessite manganese dioxides. Sol Stat Ion. 2003;159:345-356. https://doi.org/10.1016/S0167-2738(03)00035-3
22. Nguyen VH, Huynh LTN, Nguyen TH et al. Promising electrode material using Ni-doped layered manganese dioxide for sodium-ion batteries. J Appl Electrochem. 2018;48:793-800. https://doi.org/10.1007/s10800-018-1196-0
23. Tran VM, Huynh LTN, Le PPN et al. Electrochemical Na-Migration into Delithiated Phase $Li_zNi_{1/3}Mn_{1/3}Co_{1/3}O_2$: Structure and Electrochemical Properties. J Electrochem Soc. 2018;165:A1558-A1562. https://doi.org/10.1149/2.1281807jes
24. Trinh DV, Nguyen MTT, Huynh NTL et al. A Study on Crystalline Structure and Li+-Ion Diffusion Coefficient of LiNixFe1−xPO4/C Cathode Material. Arab J Sci Eng. 2023;48:7713-7720. https://doi.org/10.1007/s13369-023-07799-5